

Probabilistic modeling and global sensitivity analysis for CO₂ storage in geological formations: a spectral approach

Bilal Saad,
Alen Alexanderian,
Serge Prudhomme, and
Omar M. Knio

Received: date / Accepted: date

Abstract

This work focuses on the simulation of CO₂ storage in deep underground formations under uncertainty and seeks to understand the impact of uncertainties in reservoir properties on CO₂ leakage. To simulate the process, a non-isothermal two-phase two-component flow system with equilibrium phase exchange is used. Since model evaluations are computationally intensive, instead of traditional Monte Carlo methods, we rely on polynomial chaos (PC) expansions for representation of the stochastic model response. A non-intrusive formalism is used to determine the PC coefficients. In addition to characterizing the distributions of model observables, we compute probabilities of excess CO₂ leakage. Moreover, we consider the injection rate as an uncertain design parameter and compute an optimum injection rate that ensures risk of excess pressure buildup at the leaky well remains below acceptable levels. We also provide a comprehensive analysis of sensitivities of CO₂ leakage, where we compute the contributions of the random parameters, and their interactions, to the variance by computing first, second, and total order Sobol indices.

Bilal Saad · Omar M. Knio
King Abdullah University of Science and Technology, Division of
Computer, Electrical and Mathematical Sciences & Engineering,
4700 KAUST, Thuwal 23955-6900, Kingdom of Saudi Arabia

Bilal Saad
The Institute for Computational Engineering and Sciences, The
University of Texas at Austin, USA

Alen Alexanderian
Department of Mathematics, North Carolina State University,
Raleigh, NC, USA

Serge Prudhomme
Department of Mathematical and Industrial Engineering, École
Polytechnique de Montréal, Canada

Omar M. Knio Department of Mechanical Engineering and Materials Science, Duke University, Durham, NC 27708, USA

Keywords Carbon sequestration · Multiphase flow · Risk assessment · Parametric Uncertainty · Polynomial Chaos · Sensitivity analysis

Mathematics Subject Classification (2000) 86A05 · 65D32 · 60H35

1 Introduction

Carbon capture and storage (CCS) is an important topic related to reduction of the CO₂ pollution in atmosphere. In general, CCS is process of capture and long-term storage of CO₂. Different variants for CO₂ storage are explored, with the storage in deep underground formation such as oil fields, gas fields, abandoned mines, and saline formations being of highest interest. Various risks exist in CO₂ sequestration in deep underground formation, the most important being (i) CO₂ leakage through caprock failure, faults, abandoned wells (ii) Structural failure due to large pressure peaks, (iii) Brine displacement and infiltration into drinking water aquifers. Quantification of the risks is of ultimate importance for decision makers when evaluating the storage approaches before this technology can be implemented on a scale that can become relevant for the climate. In the scope of the deep geological storage of CO₂, there has been significant research efforts dealing with the mathematical and numerical models for simulating the CO₂ injection processes into geological formations. Nordbotten et al. [28,29,30], presented in a series of paper the development of a semi-analytical model to describe the space and time evolution of the CO₂ plume and the leakage through abandoned wells. A reduced spatial dimension models based on vertical equilibrium was discussed by Nilsen et al. [27]. Ebigbo et al. [12] set up benchmark examples for a comparison of different modelling approaches such as numerical and a semi-analytical models, for the problem of CO₂ leakage. Class et al. [9] published a benchmark study, comparing a number of mathematical and numerical models with different complexity applied to specific 3D problems in the context of CO₂ storage in geological formations.

CO₂ sequestration is a complex multiphysics process, in which multiphase multicomponent flows play a critical role. The fact that the CO₂ should be stored for many thousands of years implies that full scale experiments are not possible, and computer simulation is the main approach for exploring the feasibility of different CO₂ storage options. However the mathematical models of underground CO₂ storage involve many sources of geolog-

ical uncertainties [18,21]. These uncertainties are due to the limited knowledge about reservoir properties such as porosity and permeability. These sources of uncertainty lead to large variabilities in the predictive modeling of subsurface processes. Hence, one needs to propagate such uncertainties throughout the calculations to quantify their impact on results of computer simulations. This requires the use of stochastic modeling approaches.

Survey of literature on UQ for CO₂ storage In [32], the authors use PCEs for probabilistic analysis of the CO₂ leakage rate in the CO₂ benchmark presented by Class et al. [9]. In that article, the authors consider three uncertain parameters (reservoir porosity, reservoir permeability and fault permeability) and two design parameters (injection rate and size of screening interval), and use a number of simplifying assumptions to set up the mathematical model: fluid properties such as density and viscosity are constant, all processes are isothermal, CO₂ and brine are immiscible phases, capillary pressure is negligible and mutual dissolution is neglected. In [42] the authors utilize a stochastic response surface method for assessment of leakage detectability for CO₂ sequestration, by parametrising the spatially heterogeneous reservoir permeability using Karhunen–Loève expansion. However, the authors used the analytical solution developed by Nordbotten et al. [29] to generate pressure distribution at the injection zone, which is then used to calculate the leakage flux into a confined aquifer using Darcy’s law. The analytical solution in [29] assumes that the phase saturations and fluid viscosities are constant within each zone, the capillary effects are small, and vertical equilibrium applies to the entire flow system.

The article [43] provides estimates of the risk of brine discharge into freshwater aquifers due to CO₂ injection into geological formations and resultant salt concentrations in the overlying drinking water aquifers using arbitrary PCEs combined with the probabilistic collocation method, presented in [31]. Other efforts include [33, 34] where the authors develop a screening and ranking method and a certification framework based on effective trapping for geologic carbon sequestration, for selecting suitable storage sites on the basis of health, safety, and environmental (HSE) risk resulting from CO₂ or brine leakage. Similarities and differences between radioactive waste disposal and CO₂ storage for performance assessment have been discussed in [26]. We also mention [51] that presents a simple analytical method for the quick assessment of the CO₂ storage capacity in closed and semi-

closed systems to assess the expected pressure buildup and CO₂ storage capacity in such potentially pressure-constrained systems.

Spectral methods for uncertainty quantification (UQ) In the present work, we rely on spectral UQ methods to build a surrogate model for the nonlinear function that maps the uncertain model parameters to the model observables. In particular, we utilize polynomial chaos (PC) expansions to build such surrogates. PC expansions, whose theory goes back to late 30’s and 40’s [44,8], have become an increasingly popular tool in recent years as they provide efficient means for performing UQ in computationally intensive mathematical models; see e.g., [47,48, 49,23,25,24,32,2,3,46,50,35] for a nonexhaustive sample of research efforts on numerical methods for UQ using PC expansions and applications of these methods to real world problems.

PC methods utilize an approximation of the model variables in terms of a spectral expansion in an orthogonal polynomial basis. Once available, the PC representations can be used to efficiently approximate the statistical properties of the model outputs. Generally, there are two approaches for computing a PC expansion: (1) the intrusive method (see e.g. [47,48,49,23,25,24]) and (2) the non-intrusive method (see e.g., [4,24,2]). The intrusive method requires a reformulation of the original uncertain PDEs that govern the system, through a Galerkin projection onto the PC basis [16,22]. This entails the need for rewriting the existing deterministic solvers. Subsequently, one has to solve a larger system for the time/space evolution of the PC coefficients. Non-intrusive methods, on the other hand, provide a means to compute the spectral representation via a sampling of the existing deterministic solvers. In this paper, we will follow a non-intrusive approach to compute the coefficients in a PC expansion.

Our approach The goal of this article is to further the understanding of the impact of parametric uncertainties in the physical processes involved in CCS. This is important both to gain further insight into the uncertain response of the physical system to uncertain parameters and to enhance the predictive capabilities of a mathematical models for this physical system. In this paper, we model the fluid properties, such as density, viscosity, and enthalpy of the CO₂ and brine phases, as functions of the aquifers conditions. The reason for this is that the fluid properties are expected to change as the CO₂ rises. This will have a strong influence on the CO₂ arrival time to the leaky

well and the leakage rate value of the CO₂. Therefore, a non-isothermal two-phase two-component model is used to describe the flow processes of the leakage problem. In addition, we use nonlinear functions for the capillary pressure and the relative permeability for each phase.

We consider the uncertainties in reservoir absolute permeability, permeability of the leakage well and reservoir porosity, and in the injection rate. We begin our analysis by building a PC surrogate for CO₂ leakage rate through the leaky well. We first test the convergence of our approximation, and then, use this approximation to understand the time dependent behavior of the statistical distribution of selected quantities of interest (QoIs). We also consider the statistical response of the caprock pressure to the uncertain parameters, and devise a method for choosing an optimal injection rate that results in minimal risk of excess pressure buildup at the leaky well.

To further understand the impact of the uncertain parameters, we provide a comprehensive analysis of sensitivity of CO₂ leakage to the uncertain parameters. This is achieved by computing the Sobol indices [37, 19, 38, 36]. Traditional methods for computing the Sobol indices rely on computationally expensive sampling-based methods that require thousands of model evaluations. On the other hand, PCEs provide an efficient means to compute the Sobol sensitivity indices [11, 41, 3]. We find that all the uncertain parameters under study have a significant impact on model variability, but that the balance of sensitivity indices changes over time. We also quantify the impact of interactions between the uncertain parameters to variance. To this end, we compute second-order (joint) sensitivity indices that quantify the impact of pairwise interactions between the parameters. Moreover, to shed further light into the impact of overall interactions among uncertain parameters to the variance, we introduce a new variance-based sensitivity measure, which we call the mixed index. This mixed index, which we describe in detail below, can be computed at reasonable computational cost, once a PC surrogate is available.

Paper overview This article is structured as follows. In Section 2, we outline our model test problem, which is the benchmark problem described in [9], and describe the governing PDEs, the initial and boundary conditions, and the numerical solver used. In Section 3, we outline the requisite background material for uncertainty quantification using polynomial chaos expansions. Then, in Section 4, we present the uncertain parameters that we focus on, their distributions, and the model observables

of interest we study. Section 5 compiles our numerical results and analyzes the impact of parametric uncertainties in the physical processes involved in CO₂ storage, in the benchmark geological structure under study. Finally, we provide concluding remarks in Section 6.

2 The mathematical model

2.1 Description of the benchmark problem

We focus on the benchmark leakage problem of injected CO₂ into the aquifer through an abandoned leaky well defined by Class et al. [9]. This benchmark problem is developed based on the studies in [28, 29, 30]. It considers a leakage scenario model that consists of three hydrogeological layers (two aquifers separated by an aquitard) characterized by uniform thickness and homogeneous parameters and involving one CO₂ injection well and one leaky well. The domain's lateral dimensions are 1000 m × 1000 m. Figure 1 summarizes the geometry of the model and gives an illustration of a 2D section of the 3D domain under consideration. After being injected into the aquifer, CO₂ spreads within the aquifer and, upon reaching a leaky abandoned well, connects the two aquifers and rises to a shallower aquifer. The leaky well is at the center of the domain and the injection well is 100 m away. Both aquifers are 30 m thick and the separating aquitard (caprock) has a thickness of 100 m. We consider spatial heterogeneity only through layers according to different geological media. The leaky well is modelled as a porous medium with a higher permeability K_L than that of the formation K_A .

The benchmark problem considers the changes in fluid properties of CO₂ while rising to top aquifer. The CO₂ and brine fluid properties such as density and viscosity are dependent on the aquifer conditions, temperature T , CO₂ phase pressure p_c , brine salinity $s_{\text{salt}} = 0.1$ kg NaCl per kg and CO₂ mass fraction in brine. These changes are expected to have a strong influence on the CO₂ leakage rate.

2.2 Governing equations

The physical process of CO₂ injection in geologic reservoirs, including solubility trapping, is a non-isothermal two-phase two-component flow in porous media, which is governed by a system of coupled nonlinear partial differential equations. In this model, the water-rich phase

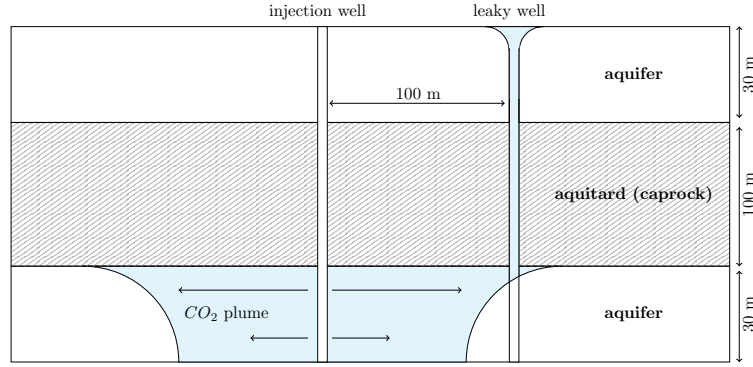


Fig. 1: Schematic view of the benchmark problem.

(brine, b) and the carbon dioxide-rich phase (CO_2 , c) consists of two components (water, w and CO_2 component, n), as the solubility of the components in the phases has to be taken into account.

Local equilibrium phase exchange of the components in the phases is assumed. Mass balance of the two components yields two partial differential equations for the components β in the phases α

$$\phi \partial_t (\rho_{\text{mol},b} \mathbf{x}_b^w S_b + \rho_{\text{mol},c} \mathbf{x}_c^w S_c) + \text{div}(\rho_{\text{mol},b} \mathbf{x}_b^w \mathbf{V}_b + \rho_{\text{mol},c} \mathbf{x}_c^w \mathbf{V}_c) + \text{div}(\mathbf{J}_b^w + \mathbf{J}_c^w) = f^w, \quad (1)$$

$$\phi \partial_t (\rho_{\text{mol},b} \mathbf{x}_b^n S_b + \rho_{\text{mol},c} \mathbf{x}_c^n S_c) + \text{div}(\rho_{\text{mol},b} \mathbf{x}_b^n \mathbf{V}_b + \rho_{\text{mol},c} \mathbf{x}_c^n \mathbf{V}_c) + \text{div}(\mathbf{J}_b^n + \mathbf{J}_c^n) = f^n. \quad (2)$$

Here, we denote by ϕ the porosity, $\rho_{\text{mol},\alpha}$ the molar density of phase α , S_α the α saturation, \mathbf{V}_α the velocity phase α , \mathbf{J}_α^β a diffusive flux of the β component into the α phase, \mathbf{x}_α^β the molar fraction of components β in phase α , f^β a source terms for the β component.

We also include the energy balance equation for thermal processes that may occur while the CO_2 migrates through the formation. Under the assumption of local thermal equilibrium, only one energy balance equation for the fluid-filled porous medium is necessary

$$\phi \frac{\partial (\sum_\alpha \rho_\alpha u_\alpha S_\alpha)}{\partial t} + (1 - \phi) \frac{\partial \rho_s c_s T}{\partial t} - \text{div}(\lambda_{\text{pm}} \nabla T) + \sum_\alpha \text{div} \{ \rho_\alpha h_\alpha \mathbf{V}_\alpha \} = f^h; \alpha \in \{b, c\}. \quad (3)$$

where ρ_α is the mass density of phase α , T is the temperature, u_α is the specific internal energy, ρ_s and c_s are

the density and the specific heat capacity of the porous medium, respectively, h_α is the specific enthalpy, f^h is the heat source term, λ_{pm} is the effective heat conductivity of the fluid-filled porous medium. The saturation of the α phases and the molar fractions (used to describe compositions of phases) satisfy

$$S_b + S_c = 1,$$

$$\mathbf{x}_b^w + \mathbf{x}_b^n = 1,$$

$$\mathbf{x}_c^w + \mathbf{x}_c^n = 1.$$

The relation between the phase pressures is given through the capillary pressure using the Brooks-Corey model [6]:

$$p_{\text{cap}}(S_b) = p_c - p_b. \quad (4)$$

The phase velocities \mathbf{V}_α are given by the extended Darcy's law for multiphase flow in porous media:

$$\mathbf{V}_b = -\mathbf{K} \frac{k_{rb}(S_b)}{\mu_b} (\nabla p_b - \rho_b \cdot \mathbf{g}), \quad (5)$$

$$\mathbf{V}_c = -\mathbf{K} \frac{k_{rc}(S_c)}{\mu_c} (\nabla p_c - \rho_c \cdot \mathbf{g}), \quad (6)$$

where \mathbf{K} denotes the absolute permeability tensor, $k_{r\alpha}$ denotes the relative permeability functions, and \mathbf{g} is the gravity vector. Following Fick's law, the diffusive flux of component β in phase α is given by

$$\mathbf{J}_\alpha^\beta = -\mathcal{D}_\alpha^\beta \rho_{\text{mol},\alpha} \nabla \mathbf{x}_\alpha^\beta, \quad \mathbf{J}_\alpha^w + \mathbf{J}_\alpha^n = 0, \quad (7)$$

where \mathcal{D}_α^β is the diffusion coefficient of component β in phase α .

To close the system, supplementary constraints for mole fractions, viscosity, and density are needed. The fluid properties of CO_2 are calculated as functions of

Parameter	Value/function
CO ₂ mass density, ρ_c	$f(T, p_c)$ [39]
Brine mass density, ρ_b	$f(T, p_b, s_{\text{salt}}, x_b^n)$ [15]
CO ₂ viscosity, μ_c	$f(T, p_c)$ [13]
Brine viscosity, μ_b	$f(T, s_{\text{salt}})$ [5]
CO ₂ enthalpy, h_c	$f(T, p_c)$ [39]
Brine enthalpy, h_b	$f(T, p_b, s_{\text{salt}}, x_b^n)$ [15]
Mutual solubilities, x_{α}^{β}	$f(T, s_{\text{salt}}, p_c)$ [40]
Brine salinity, s_{salt}	0.1 kg NaCl per kg
Residual brine saturation, S_{rb}	0.2
Residual CO ₂ saturation, S_{rc}	0.05
Relative permeability, $k_{r\alpha}$	Brooks and Corey [6]
Capillary pressure, $p_{\text{cap}}(S_b)$	Brooks and Corey [6]
Entry pressure, P_e	10 ⁴ Pa
Brooks-Corey parameter, λ	2.0
Leaky & injection well radius	0.15 m

Table 1: Fluid properties and simulation parameters.

pressure and temperature. The properties of brine additionally depend on the salinity and on the mole fraction of CO₂ in brine. Detailed information on dependencies of the fluid properties is given in Table 1.

2.3 Simulation scenario

For computational efficiency, only the aquifers and the leaky well are discretized, as the aquitard is a layer of impermeable rock. The boundaries between the meshed regions and the aquitard are taken to be no-flow boundaries. The initial conditions in the domain include a hydrostatic pressure distribution which is dependent on the brine density and a geothermal temperature distribution dependent on the geothermal gradient. The geothermal gradient is assumed to be 0.03 K/m and the initial temperature at the bottom (at 3000 m depth) is 100°C. The aquifers are initially saturated with brine. The initial pressure at the bottom of the domain equal 3.086×10^7 Pa. The lateral boundary conditions are constant Dirichlet conditions and equal to the initial conditions. At the top and bottom of the domain, there are no-flow boundary conditions for both brine and CO₂.

In the benchmark setup, CO₂ is injected at a constant rate of 8.87 kg/s, which corresponds to 1600 m³ per day at reservoir conditions. The total simulation time is 2000 days. All relevant parameters used for the simulation are given in Table 1. For more details we refer to [9].

The CO₂ leakage rate (denoted by Q_{leak} in this paper) the output quantity of interest (QoI) of the benchmark study, is defined as the total CO₂ mass flow at midway

between the top and bottom aquifers divided by the injection rate, in percent.

The DuMuX simulator [14] was employed to solve (1)–(7) using the so-called Box method [20] for spatial discretization, which is a vertex-centered finite volume method and the implicit Euler scheme is applied for the temporal discretization. DuMuX is a multi-scale multi-physics toolbox for the simulation of flow and transport processes in porous media. It provides a framework for easy and efficient implementation of models for porous media flow problems, ranging from problem formulation, selection of spatial and temporal discretisation schemes, as well as non-linear solvers, to general concepts for model coupling.

3 Background on spectral methods for uncertainty quantification

We begin our discussion of spectral UQ methods, by using the problem of uncertainty quantification for CO₂ leakage, which we denote by $Q_{\text{leak}} = Q_{\text{leak}}(\mathbf{x}, t, \mathbf{q})$ where \mathbf{x} is a spatial point and t denotes time. The vector \mathbf{q} contains a set of parameters defining various physical properties of the system. These parameters appear as coefficients, or boundary or volume forcing terms in the governing PDEs. Any of the elements of this vector are, in practice, not known exactly and are hence considered uncertain. An important consideration in obtaining high-fidelity predictions is to quantify the impact of these parametric uncertainties in the model observables such as Q_{leak} . To this end, we model the uncertain parameters as random variables that are parameterized by a vector $\boldsymbol{\theta}$ of canonical random variables. Hence, we will have $Q_{\text{leak}} = Q_{\text{leak}}(\mathbf{x}, t, \mathbf{q}(\boldsymbol{\theta}))$. The random vector $\boldsymbol{\theta}$ fully characterizes the uncertain parameter vector \mathbf{q} and, therefore, we can unambiguously use the simpler notation $Q_{\text{leak}}(\mathbf{x}, t, \boldsymbol{\theta})$ for the uncertain CO₂ leakage, a convention which we follow for the other uncertain model variables below as well.

Below we seek to approximate the nonlinear mapping $\boldsymbol{\theta} \mapsto Q_{\text{leak}}(\mathbf{x}, t, \boldsymbol{\theta})$ through a spectral representation of the form

$$Q_{\text{leak}}(\mathbf{x}, t, \boldsymbol{\theta}) = \sum_{k=0}^{\infty} c_k(\mathbf{x}, t) \Psi_k(\boldsymbol{\theta}),$$

where the Ψ_k 's form a orthogonal basis in an appropriate Hilbert space (discussed below), and $c_k(\mathbf{x}, t)$ are expansion coefficients. Such a spectral representation can then

be used as a cheap-to-evaluate *surrogate* for the parameter-to-observable map, $\theta \mapsto Q_{\text{leak}}(x, t, \theta)$. This enables efficient methods for characterizing the uncertainties in Q_{leak} that replace expensive PDE solves by cheap evaluations of the surrogate.

3.1 Notation and definitions

We denote by $(\Omega, \mathcal{F}, \mu)$ a probability space, where Ω is the sample space, \mathcal{F} is an appropriate σ -algebra on Ω , and μ is a probability measure. For a random variable θ on Ω , we write $\theta \sim \mathcal{U}(a, b)$ to mean that θ is uniformly distributed on the interval $[a, b]$ and $\theta \sim \mathcal{N}(0, 1)$ to mean that θ is a standard normal random variable. We use the term iid for a collection of random variables to mean that they are independent and identically distributed. The distribution function of a random variable θ on Ω is given by $F_\theta(x) = \mu(\theta \leq x)$ for $x \in \mathbb{R}$.

In the present work, we consider models with finitely many uncertain parameters. We parameterize these uncertain parameters by a finite collection of real-valued independent random variables $\theta_1, \dots, \theta_d$ that are defined on Ω . We let F_θ denote the joint distribution function of the random vector $\theta = (\theta_1, \dots, \theta_d)^T$. Since the θ_i are independent, $F_\theta(x) = \prod_{i=1}^d F_i(x_i)$ for $x \in \mathbb{R}^d$, where F_i is distribution function of the i th coordinate.

The random vector θ takes values in \mathbb{R}^d . In fact, it is sufficient to consider the subset Θ of \mathbb{R}^d given by the support of the distribution function F_θ . Following common practice, we work in the image probability space $(\Theta, \mathcal{B}(\Theta), F_\theta)$, where $\mathcal{B}(\Theta)$ is the Borel σ -algebra on Θ (which is a standard choice). For notational convenience we suppress $\mathcal{B}(\Theta)$ below and denote the image probability space by (Θ, F_θ) . We denote the expectation of a random variable $X : \Theta \rightarrow \mathbb{R}$ by

$$\langle X \rangle = \int_{\Theta} X(s) F_\theta(ds).$$

The space of square-integrable random variables on Θ , $L^2(\Theta, F_\theta)$, is endowed with the inner product (\cdot, \cdot) defined by $(X, Y) = \int_{\Theta} X(s)Y(s)F_\theta(ds) = \langle XY \rangle$, and the corresponding induced norm $\|\cdot\| = (\cdot, \cdot)^{1/2}$.

3.2 Polynomial chaos expansion

In the case $\theta_i \stackrel{\text{iid}}{\sim} \mathcal{N}(0, 1)$, for $i = 1, \dots, d$, any $X \in L^2(\Theta, F_\theta)$ admits an expansion of the form,

$$X = \sum_{k=0}^{\infty} c_k \Psi_k, \quad (8)$$

where $\{\Psi_k\}_0^\infty$ is a complete orthogonal set consisting of d -variate Hermite polynomials, and the series converges in $L^2(\Theta, F_\theta)$. The infinite series representation of X is known as the polynomial chaos (PC) or Wiener–Hermite expansion of X [44, 8, 16, 22]. The Wiener–Hermite expansion is the appropriate choice in the case the model parameters are parameterized by normally distributed random variables. In the case where the sources of uncertainty follow other distributions, alternative parameterizations and polynomial bases are adopted [22]. For example, in the case where $\theta_i \stackrel{\text{iid}}{\sim} \mathcal{U}(-1, 1)$ the appropriate PC basis is given by the d -variate Legendre polynomials.

Tensor product construction of a multivariate PC basis

Let $\theta = (\theta_1, \dots, \theta_d)$, where θ_i are independent random variables that are distributed according to common choices given by standard normal, uniform, or beta distributions. We work with a multivariate PC basis that is obtained through a tensor product of appropriate one-dimensional bases. More precisely, if we denote by $\{\psi_j(\theta_i)\}_{j=1}^\infty$ the one-dimensional orthogonal polynomial basis corresponding to θ_i (with the choice of basis dictated by the distribution of θ_i), we form the multivariate PC basis $\{\Psi_k\}_{k=0}^\infty$ as follows:

$$\Psi_k(\theta) = \prod_{i=1}^d \psi_{\alpha_i^k}(\theta_i), \quad \theta \in \Theta, \quad (9)$$

where $\alpha^k = (\alpha_1^k, \alpha_2^k, \dots, \alpha_d^k)$ is a multi-index, and α_i^k indicates the order of the 1D polynomials in θ_i . For example, if θ_i is standard normal, then $\psi_{\alpha_i^k}$ is the Hermite polynomial of order α_i^k . With this basis, any $X \in L^2(\Theta, F_\theta)$ admits an expansion of the form: $X = \sum_{k=0}^\infty c_k \Psi_k$, which is known as the generalized polynomial chaos expansion of X . In computer implementations, we will approximate $X(\theta)$ with a truncated series,

$$X(\theta) \approx \sum_{k=0}^P c_k \Psi_k(\theta) \quad (10)$$

where P is specified based on the choice of truncation strategy. In the present work, we consider truncations

based on the total degree of the polynomials in the series. In this case, letting p be the largest (total) polynomial degree allowed in the expansion, it is straightforward to show that $P = (d + p)! / (d! p!) - 1$, where as before d is the dimension of the uncertain parameter vector θ .

Note that with X expanded as in (10), using the orthogonality of the basis $\{\Psi_k\}_0^P$ and the convention that $\Psi_0 = 1$, we have immediate access to its first and second moments:

$$\langle X \rangle = c_0, \quad \langle X^2 \rangle = \sum_{k=0}^P c_k^2 \langle \Psi_k^2 \rangle,$$

from which we also get $\text{var}\{X\} = \sum_{k=1}^P c_k^2 \langle \Psi_k^2 \rangle$.

Tests of convergence To assess accuracy of a PC expansion, one could begin by studying convergence in distribution. A practical method of doing this is by tracking the probability density function (pdf) of the PC expansion (which can be approximated efficiently by sampling the expansion and using for example a Kernel Density Estimation (KDE) method) as the order of the expansion is increased. Moreover, to get further confidence in the spectral representation of a random variable $X(\theta)$, one can use the relative L^2 error, E_{rel} , between X and its truncated PC representation:

$$E_{\text{rel}}^2 := \frac{\int_{\Theta} |X(s) - \sum_{k=0}^P X_k \Psi_k(s)|^2 F_{\theta}(ds)}{\int_{\Theta} |X(s)|^2 F_{\theta}(ds)}, \quad (11)$$

which can be approximated using either quadrature or sample averaging.

3.3 Non-intrusive spectral projection

Let X belong to $L^2(\Theta, F_{\theta})$. As mentioned in the introduction, non-intrusive methods aim at computing the PC coefficients in the finite expansion (10) via a set of deterministic evaluations of $X(\theta)$ for specific realizations of θ . Observe that since $\{\Psi\}_0^P$ form an orthogonal system, we have: $\langle X, \Psi_k \rangle = \left(\sum_{l=0}^P c_l \langle \Psi_l, \Psi_k \rangle \right) = \sum_{l=0}^P c_l \langle \Psi_l, \Psi_k \rangle = c_k \langle \Psi_k, \Psi_k \rangle$, so that the coefficient c_k is given by

$$c_k = \frac{\langle X, \Psi_k \rangle}{\langle \Psi_k^2 \rangle}.$$

The moments $\langle \Psi_k^2 \rangle$ of known orthogonal polynomials can be computed analytically, and hence, the determination of coefficients c_k amounts to the evaluation of the

moments $\langle X \Psi_k \rangle$. In the non-intrusive spectral projection (NISP) approach, these moments are approximated via quadrature:

$$\langle X \Psi_k \rangle = \int_{\Theta} X(s) \Psi_k(s) F_{\theta}(ds) \approx \sum_{j=1}^{N_q} \omega_j X(\theta^{(j)}) \Psi_k(\theta^{(j)}),$$

where $\theta^{(j)} \in \Theta$ and ω_j are the nodes and weights of an appropriate quadrature formula. Note that in this formulation, the same set of nodes is used to compute all coefficients c_k . Hence, the complexity of NISP, measured in the number of evaluations of $X(\theta)$ (i.e., the number of model solves), scales with the number of quadrature nodes N_q . These multi-dimensional quadrature rules are constructed by full or partial tensorization of one-dimensional quadrature formulas. Therefore, the number N_q of quadrature nodes scales with the dimension of the uncertain parameter—a phenomenon commonly referred to as the curse of dimensionality. In the present work, we work with a small number of uncertain parameters, and hence a full-tensor Gaussian quadrature was found feasible. However, for higher-dimensional problems, sparse grids, or adaptive sparse grids are more suitable [22, 46].

We remark that the efficient construction of PC expansions via non-intrusive methods has resulted in significant research activity in recent years. The efforts include adaptive pseudo-spectral projections [10, 7] as well as regression-based approaches that incorporate sparsifying penalty methods [17, 50, 35]. While the goal of the present work is not the study of such methods, nor their extensions, we point them out as potential solutions for the problems with higher-dimensional parameters, where one seeks to utilize PC expansions for uncertainty analysis.

3.4 Variance-based sensitivity analysis

An important step in quantifying the impact of parametric uncertainties on the response of an uncertain system is that of parametric sensitivity analysis. In particular, global or variance-based sensitivity analysis [37, 19, 38, 36] enables the characterization of the contribution of the individual uncertain parameters or their interactions to the total variance of the model response. In this section we outline the concepts from variance-based sensitivity analysis that are used in the present work.

Consider a square-integrable random variable $X(\theta)$. The first-order (or main effect) sensitivity indices quantify the effect of the i^{th} coordinate θ_i alone on the vari-

ance of the random variable $X(\boldsymbol{\theta})$. These first-order indices, which we denote by SS_i , are defined as follows,

$$SS_i = \frac{\text{var}\{E\{X(\boldsymbol{\theta})|\theta_i\}\}}{\text{var}\{X(\boldsymbol{\theta})\}}, \quad i \in \{1, \dots, d\}. \quad (12)$$

Here $E\{X(\boldsymbol{\theta})|\theta_i\}$ denotes the conditional expectation [45] of $X(\boldsymbol{\theta})$ given θ_i . While the mathematical definition of the first-order indices (and higher-order indices discussed below) are given in terms of conditional expectations, whose numerical approximations involve expensive sampling (see e.g., [38]), their computation via PC expansion is straightforward and very efficient [11, 41, 3, 1].

We also point out the second-order sensitivity indices that describe joint effects. Specifically, for $i, j \in \{1, \dots, d\}$, we denote by SS_{ij} the sensitivity index that quantifies the contribution of the *interaction* between θ_i and θ_j to the total variance. The mathematical definition of SS_{ij} is as follows,

$$SS_{ij} = \frac{\text{var}\{E\{X(\boldsymbol{\theta})|\theta_i, \theta_j\}\}}{\text{var}\{X(\boldsymbol{\theta})\}} - (SS_i + SS_j). \quad (13)$$

Higher-order joint sensitivity indices (for example SS_{ijk}) can be defined also, but usually are not used in applications. However, in our numerical computations below we will discuss a sensitivity index, which we call the *mixed index*, that quantifies the contribution of *all* interactions among uncertain parameters.

Another useful variance based sensitivity measure is the *total sensitivity index* [19, 36]. The total sensitivity index due to θ_i is defined by,

$$T_i = \frac{\text{var}\{X(\boldsymbol{\theta})\} - \text{var}\{E\{X(\boldsymbol{\theta})|\boldsymbol{\theta}^{[-i]}\}\}}{\text{var}\{X(\boldsymbol{\theta})\}} \quad (14)$$

where $\boldsymbol{\theta}^{[-i]}$ denotes the random vector $\boldsymbol{\theta} = (\theta_1, \dots, \theta_d)$ with θ_i removed: $\boldsymbol{\theta}^{[-i]} := (\theta_1, \dots, \theta_{i-1}, \theta_{i+1}, \dots, \theta_d)$. Notice that the numerator in (14) is the total variance minus the variance of the conditional expectation $E\{X(\boldsymbol{\theta})|\boldsymbol{\theta}^{[-i]}\}$. Thus, T_i is the total contribution of θ_i , by itself and through its interactions with other coordinates, to the variance.

4 Uncertain parameters and quantities of interest

In the present study, we study the effect of uncertainties in reservoir porosity ϕ , reservoir absolute permeability K_A and permeability of the leakage well K_L on the model response. To support decision-making based on the approach presented here, we also consider one design parameter, the CO₂ injection rate Q_{CO_2} . This will help to

Table 2: Distributions of the uncertain parameters.

Parameter	Distribution
log-porosity	$\mathcal{N}(-1.8971, 0.2^2)$
log-absolute permeability	$\mathcal{N}(-30.002, 1.2^2)$
log-leakage permeability	$\mathcal{N}(-27.631, 0.3679)$
log-injection rate	$\mathcal{N}(2.1827, 0.2^2)$

study the influence of the injection rate on the CO₂ leakage rate. As reflected in Table 2 all uncertain parameters are modeled as log-normal. The distributions were adopted based on the setup in [21, 32].

In the analysis below, we focus on the following model observables that characterize the flow: (a) the CO₂ leakage through the leaky well as a function of time, (b) arrival time of the CO₂ plume at the leaky well, (c) the maximum leakage ratio, and (d) the corresponding time; these quantities are denoted, respectively, by Q_{leak} , t_{arrival} , $Q_{\text{leak}}^{\text{max}}$, and t_{maxleak} . Note that here the CO₂ leakage rate is defined as in the benchmark study as the CO₂ mass flux, in percent, at midway between top bottom aquifer divided by the injection rate. We also aim to understand the effect of model uncertainties on the spatially distributed pressure and saturation as functions of time.

5 Analysis of uncertainties in CO₂ storage

In our computations, we used NISP based on a fully tensorized Gauss-Hermite quadrature to compute the spectral expansion of the model output in the PC basis. We used four nodes in each stochastic dimension, resulting in an ensemble of 256 model evaluations that were run on a 20-core Intel Xeon E5-2680 v2 (2.80GHz) workstation. The computational time for a single simulation run was about 18 hours using five cores. Our choice of quadrature supports a third order PC expansion, which was found to provide sufficient accuracy for the statistical tests needed in our computations.

5.1 Analyzing uncertain response of CO₂ leakage

In Figure 2, we plot the realizations of Q_{leak} as a function of time. These realizations are obtained by 256 model solves with the parameter values set according to the 256 nodes of the Gauss-Hermite quadrature. To understand the solution behavior better, in Figure 3 we report the sample mean of the CO₂ realization with the averaging done over the realizations computed at the quadrature

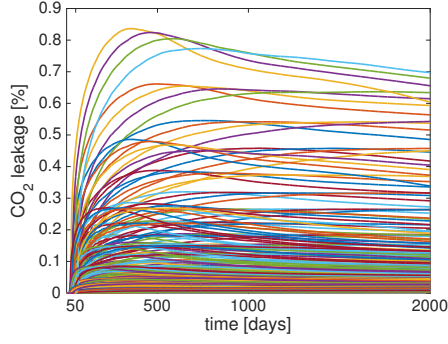


Fig. 2: Evolution of CO₂ leakage rate. The curves depict the 256 realizations corresponding to the quadrature points in the uncertain parameter space.

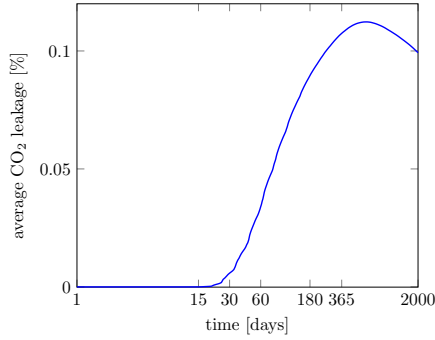


Fig. 3: Sample mean of the CO₂ leakage rate over time (averaged over realizations computed at quadrature nodes).

points. Note that in that figure, we have used a log scale for the horizontal axis to provide a clearer picture of the dynamics of CO₂ at the early times.

To obtain a PC representation of CO₂ leakage, we first project the log of CO₂ leakage in a PC basis,

$$\log Q_{\text{leak}}(t, \theta) \approx \sum_{k=0}^P c_k(t) \Psi_k(\theta).$$

The response surface for Q_{leak} can then be constructed using

$$Q_{\text{leak}}(t, \theta) \approx \exp \left(\sum_{k=0}^P c_k(t) \Psi_k(\theta) \right). \quad (15)$$

This log-projection, in particular, ensures the positivity of Q_{leak} . Figure 4 shows instantaneous distributions of CO₂ leakage rate. These distributions are obtained by sampling the PC-based surrogate model (15) at selected times. As seen in the plots, the distributions seem to level

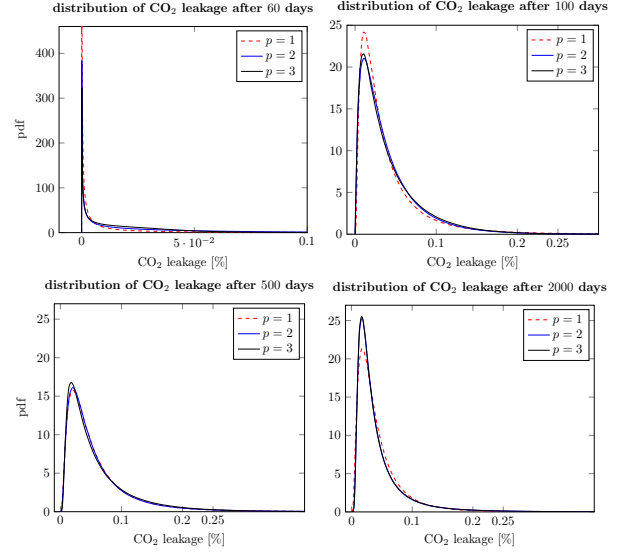


Fig. 4: Distribution of CO₂ leakage at selected times. p denotes the highest polynomial degree in the truncated expansion. In each case, the PC expansion was sampled 10^6 times to generate the distribution curve.

off as the PC order is increased to $p = 3$ suggesting that a third-order expansion is sufficient.

To further illustrate the evolution of the distribution of CO₂ leakage over time, we show in Figure 5 box plots indicating quartiles and the high probability regions of support of the distributions over time. As before, these plots are generated by sampling the PC representation of CO₂ leakage with a Monte Carlo sample size of 10^6 . These results further illustrate the skewed distribution of CO₂ leakage and its spread.

To get a more complete picture of the response of the model to parametric uncertainties, we use spectral representations to approximate the (uncertain) arrival time of the CO₂ plume at the leaky well (which is defined as the time at which the leakage value is greater than $3.0 \times 10^{-3}\%$), the maximum leakage ratio and the corresponding time; see Figure 6. Using our computed distribution of the arrival time, seen in Figure 6(left), we found that the probability of arrival time being at or before $t = 120$ is greater than 98%. Note that the use of nonlinear relative permeability-saturation relation implies that the sum of the relative permeability values of the brine and CO₂ phases is less than unity for most saturations which leads to an overall reduced mobility of the flow and thus to a reduced leakage at early times with later arrival and

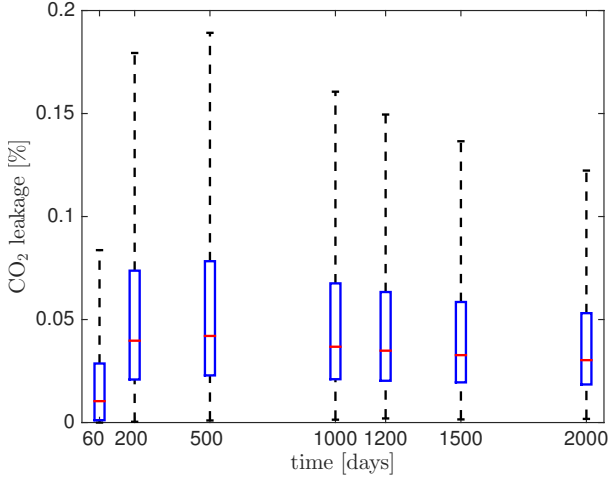


Fig. 5: Box plots depicting distribution of CO₂ leakage over time.

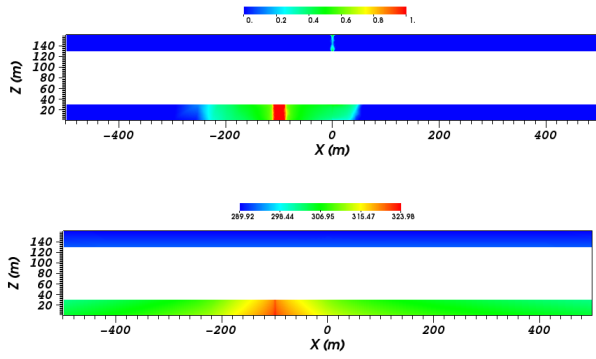


Fig. 7: A typical realization of CO₂ saturation (top), and a typical realization of pressure (bottom) at 120 days.

lower peak as the leakage rate does not rise as high as in the case of linear relative permeability [30].

There are further effects contributing to the later arrival time of CO₂ at the leaky well like increased the influence of the viscous forces in the system due to the lower relative permeabilities, compared to buoyancy due to density differences, which makes the shape of the plume become more cylindrical [21] (see Figure 7 (top) that illustrates the saturation of CO₂ after 120 days, obtained for one realization model). Figure 7 corresponds to a vertical slice through the middle of the domain. In that figure (bottom image), we also show a typical realization of the pressure field along the same vertical slice.

As a result of the increased overall resistance to the flow, the leakage rate rises smoothly when the CO₂ reaches

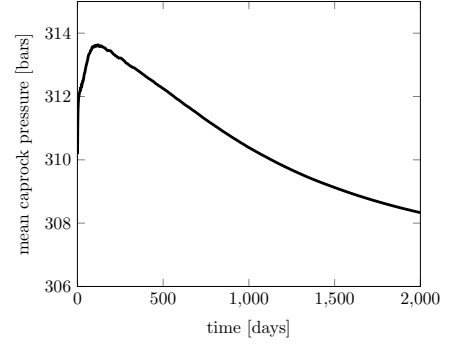


Fig. 8: Mean caprock pressure as a function of time.

the well and then approaches steady-state as a result of the boundary conditions in the benchmark description. This steady-state can be attributed to the lateral boundary conditions that influence the pressure in the domain. In Figure 8, we report the time evolution of the mean caprock pressure, where we see a reduced pressure over time. This is the reason for the leakage rate to start decreasing after the peak of the arrival of the CO₂ flux at the leaky well [30].

5.2 Long-time accuracy of the predictions of CO₂ leakage

The accuracy of our spectral representations, so far, have been examined by looking at the convergence of the pdfs, indicating convergence in distribution. To further examine the accuracy of the spectral representation of CO₂ leakage, especially for long time predictive purposes, we approximate relative L^2 errors following (11). Figure 9 shows the evolution of the L^2 errors for $t > 120$, at which time, as mentioned before, over 98% of realizations of the model output indicate arrival of CO₂ plume to the leaky well. We note that after the initial transient regime, the error for the third order PC expansion falls below one percent. This further highlights the utility of the PC expansions in building an accurate surrogate model for CO₂ leakage that is useful for making long-time predictions.

5.3 Estimating probability of excess CO₂ leakage

An important consideration in modeling CO₂ leakage in reservoirs is understanding the likelihood of excess CO₂ leakage. In particular, we consider the probability,

$$P_{\text{excess leakage}}(t) := \text{prob}(Q_{\text{leak}}(t, \theta) > L_{\text{max}}),$$

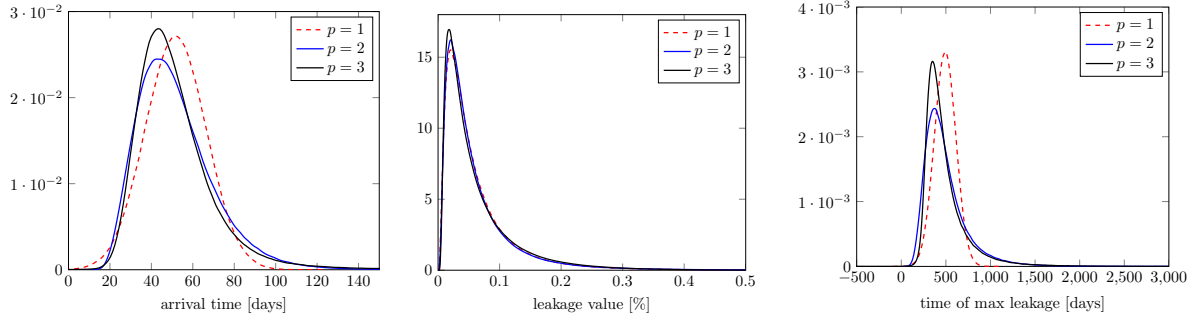


Fig. 6: Distribution of the arrival time of the CO₂ plume at the leaky well, the maximum leakage ratio and the corresponding time of the maximum leakage ratio. p in the legend denotes the highest polynomial degree in the truncated expansion. In each case, the PC expansion was sampled 10^6 times to generate the distribution curve.

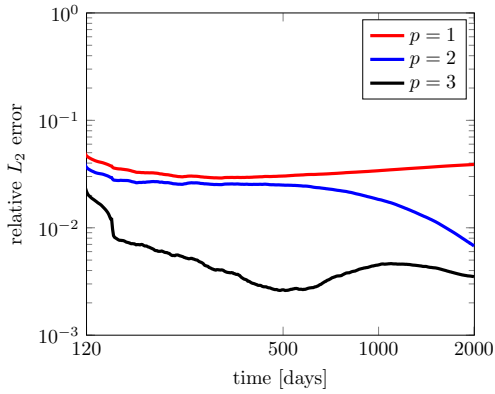


Fig. 9: Evolution of L^2 error for the log-CO₂ leakage.

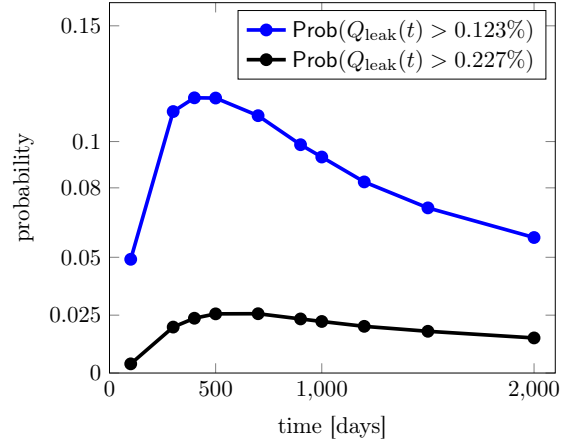


Fig. 10: Probability of excess leakage, as defined by leakage exceeding 0.123% (blue) and 0.227% (black), over time.

over time. Notice that computing such a probability is in general a computationally expensive task. However, using the cheap-to-evaluate PC representation of Q_{leak} enables estimation of such probabilities at negligible computational cost. Below we use $L_{\text{max}} = 0.123\%$ and $L_{\text{max}} = 0.227\%$, which correspond, respectively, to the maximum leakage ratio obtained in the benchmark study of CO₂ leakage through an abandoned well [9] using a simplifying assumptions to reduce the complexity of the equations and to that obtained by the more physical detailed equations used also in our study. Figure 10 depicts the time-dependent behavior of $P_{\text{excess leakage}}(t)$. These results indicate that given our assumed statistical model for the uncertain parameters, the probability of Q_{leak} exceeding 0.227% remains below 5%, but probability of Q_{leak} exceeding 0.123% reaches values of more than 10%.

5.4 Choosing optimum design to reduce risk of failure

Here we consider the caprock pressure at a point near the leaky well, and denote this quantity by $p_{\text{caprock}}(t, \theta)$. Let us consider the quantity,

$$p_{\text{caprock}}^{\infty}(\theta) = \lim_{t \rightarrow \infty} p_{\text{caprock}}(t, \theta).$$

In our numerical computations, we approximate $p_{\text{caprock}}^{\infty}$ by our computed value of the caprock pressure at the final simulation time. We define a failure probability as that of $p_{\text{caprock}}^{\infty}$ exceeding a critical caprock pressure equal to 330 bar. An optimal injection rate is the largest injection rate for which the failure probability remains below 5 percent. To define this quantity mathematically, we de-

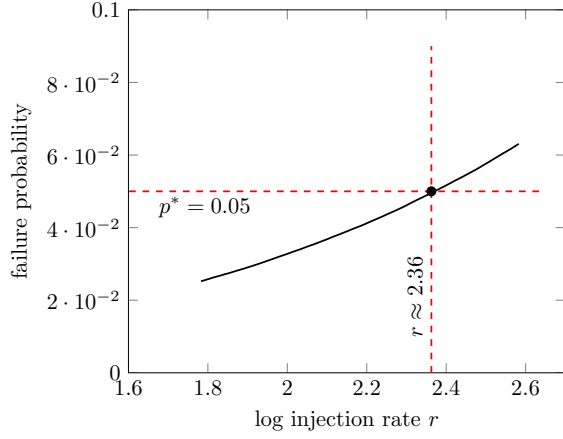


Fig. 11: Curve showing $\Pi_{\text{fail}}(r)$ as a function of r . We notice that $r \approx 2.36$ gives the largest log-injection rate (which translates to an injection rate of approximately 10.6 kg/s) that results in probability of failure being less than 5%.

note

$$\Pi_{\text{fail}}(Q_{\text{CO}_2}) := \text{Prob}(p_{\text{caprock}}^{\infty}(\theta_1, \theta_2, \theta_3; \theta_4(Q_{\text{CO}_2})) > 330),$$

with

$$\theta_4(Q_{\text{CO}_2}) = (Q_{\text{CO}_2} - \bar{Q}_{\text{CO}_2}) / \sigma_{Q_{\text{CO}_2}},$$

where \bar{Q}_{CO_2} and $\sigma_{Q_{\text{CO}_2}}$ are the mean and standard deviation of Q_{CO_2} chosen according to Table 2. Note that to compute $\Pi_{\text{fail}}(Q_{\text{CO}_2})$ at a given rate Q_{CO_2} , we use the PC surrogate for $p_{\text{caprock}}^{\infty}$, fix θ_4 at $\theta_4(Q_{\text{CO}_2})$ and, considering $p_{\text{caprock}}^{\infty}$ as a function of $\theta_1, \theta_2, \theta_3$, compute the probability $p_{\text{caprock}}^{\infty} > 330$ bar using Monte Carlo Sampling, which can be done very efficiently using the PC surrogate. Then, we define the optimum injection rate $Q_{\text{CO}_2}^*$ according to

$$Q_{\text{CO}_2}^* = \max_{Q_{\text{CO}_2}} \{Q_{\text{CO}_2} : \Pi_{\text{fail}}(Q_{\text{CO}_2}) < 0.05\}.$$

Figure 11 illustrates the choice of the injection rate based on a critical caprock pressure equal to 330 bar after 2000 days. The results in Figure 11 indicate that the maximum injection rate where the caprock pressure does not exceed the limit of 330 bar is approximately 10.6 kg/s.

5.5 Global sensitivity analysis

In reservoir modeling, porosity and permeability are the most important petrophysical parameters. In this section,

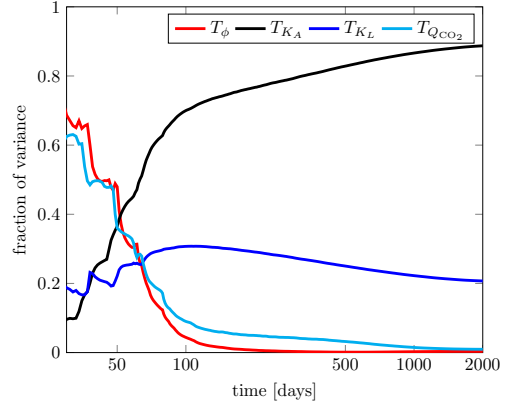


Fig. 12: Total sensitivity indices over time.

we analyze the importance of each of the uncertain parameters to the uncertainties in the CO_2 leakage. To this end, we perform a variance-based sensitivity analysis, where we find how much each uncertain input parameter contributes to the total variance in CO_2 leakage.

Figure 12 depicts the time-dependent behavior of total sensitivity indices for CO_2 leakage. For clarity, we denote the total sensitivity indices for the random inputs by T_{ϕ} , T_{K_A} , T_{K_L} , and $T_{Q_{\text{CO}_2}}$, corresponding to total sensitivity index for porosity, reservoir permeability, leaky well permeability and CO_2 injection rate. The results in Figure 12 indicate that at early time, the porosity and the CO_2 injection rate have a significant influence onto the total variance. However, as the flow reaches the fault, the variance of CO_2 becomes dominated by the uncertainties in K_A and K_L .

To further understand the contribution of the different uncertain parameters to variability in CO_2 leakage, we also consider the first-order indices S_{ϕ} , S_{K_A} , S_{K_L} , and $S_{Q_{\text{CO}_2}}$ in Figure 13 and the second-order indices that show the contribution of the interaction between random parameters to the total variance in Figure 14. We note that at early times the interactions between the uncertain parameters have a noticeable contribution to the total variance, but as the time passes the second-order interactions mostly vanish (except the interaction between K_A and K_L) and the first-order indices are almost equal to the total indices reported in Figure 12. That is, as the CO_2 plume reaches the leaky well the response of the system becomes nearly additive in the uncertain parameters.

To quantify the total contribution of the interactions between uncertain parameters to the variance of model output (CO_2 leakage in the present case), we consider

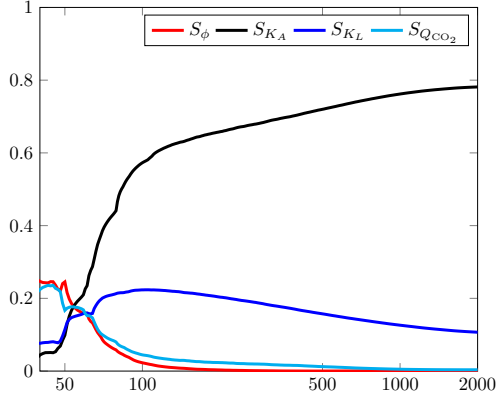


Fig. 13: First-order sensitivity indices over time.

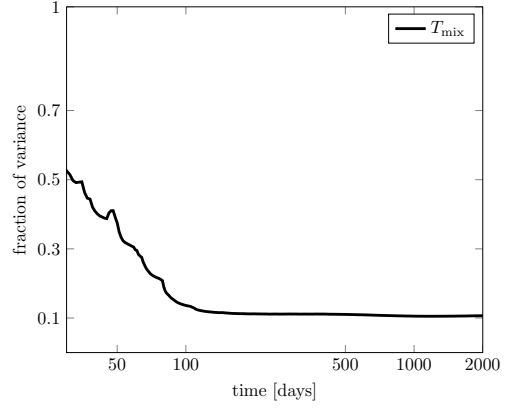
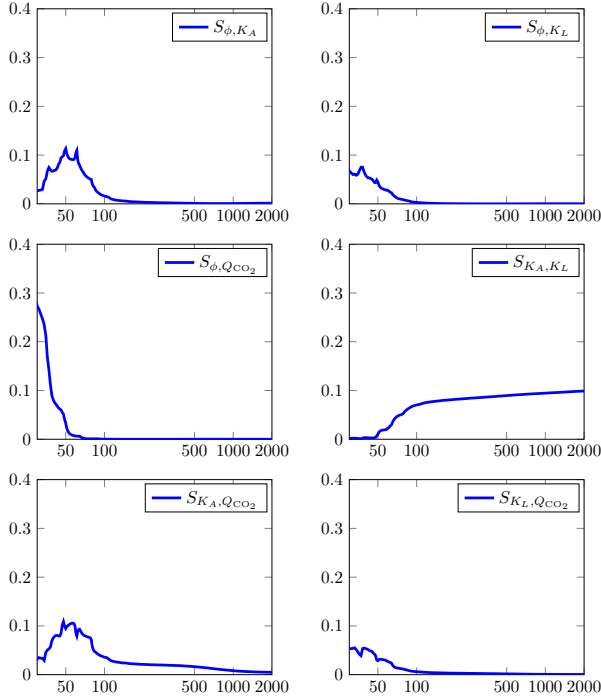
Fig. 15: The mixed sensitivity index T_{mix} over time.

Fig. 14: Second-order sensitivity indices over time.

the following *mixed sensitivity index*,

$$T_{\text{mix}} := \frac{\text{variance due to interactions between parameters}}{\text{total variance}}.$$

This mixed index can be defined in terms of conditional expectations (cf. Section 3.4), and is general difficult to approximate. However, using the PC representation of the model response (CO₂ leakage here), we can easily derive the following expression for T_{mix} . Using the multi-index construction of the multivariate PC basis in (9), we

can define,

$$T_{\text{mix}} \approx \frac{\sum_{k \in \mathcal{K}} c_k^2 \|\Psi_k\|_{L^2(\Omega)}^2}{\sum_{k=1}^P c_k^2 \|\Psi_k\|_{L^2(\Omega)}^2},$$

where the index set \mathcal{K} is defined by

$$\mathcal{K} = \{k \in \{1, \dots, P\} : \|\alpha_k\|_0 > 1\}.$$

Note that here we have used the multi-index notation, used in construction of the PC basis, and denoted by $\|\cdot\|_0$ the ℓ_0 -“norm”. That is, for a vector x , $\|x\|_0$ is the number of nonzero elements of x .

The index T_{mix} quantifies the contribution to the variance due to all interactions (second and higher order) between the uncertain inputs. Using the third-order PC expansion we have computed for CO₂ leakage, we approximate the mixed index for this QoI; see Figure 15. The results reported in Figure 15 show that, as also seen from the study of first- and second-order indices, there is significant contributions to model variability coming from interactions between the parameters at early times. These mixed-effect interactions level off at around 10% as the CO₂ plume reaches the leaky well.

Finally, we compute the sensitivity indices over the three-dimensional computational domain. In particular, we consider the sensitivity of CO₂ saturation to the uncertain inputs. Figure 16 shows the spatial distribution of the total sensitivity indices, T_ϕ and T_{K_A} for CO₂ saturation at $t = 70$ days. A vertical slice through the middle of the domain indicates that the regions where porosity has a significant contribution to variance travel with the fronts of the CO₂ plume, whereas the reservoir permeability maintains a nearly constant dominant effect on variance within the regions with high CO₂ saturation.

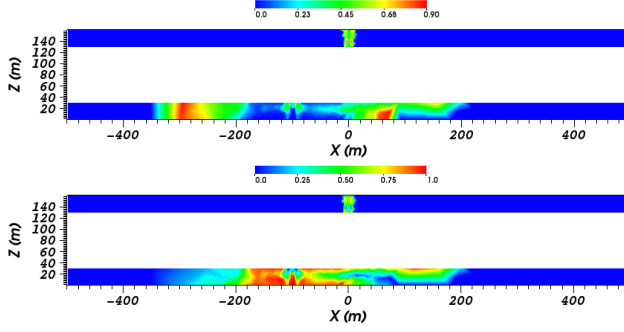


Fig. 16: Space propagation of sensitivities after 70 days. Here we consider the sensitivity of saturation to porosity ϕ (top) and reservoir permeability (bottom).

6 Conclusions and Summary

A non-intrusive spectral projection approach was implemented to propagate and quantify parametric uncertainties for CO₂ storage in geological formations using a common 3D leakage benchmark problem of injected CO₂ into overlying formations through a leaky well. A non-isothermal two-phase two-component flow system with equilibrium phase exchange is used. Moreover, we use nonlinear functions for the capillary pressure and the relative permeability for each phase.

In our numerical results, we find that the use of a nonlinear relative permeability-saturation relation in our mathematical model leads to an overall reduced mobility of the flow. This behavior is seen in the statistical distribution of the CO₂ arrival time to the leaky well. In particular, tracking the time evolution of the distribution of the CO₂ leakage, we see that the leakage rate to start decreasing after the peak of the arrival of the CO₂ flux at the leaky well. This is in contrast with the cases where one uses simplified assumptions such as linear relative permeabilities, which decreases the influence of the viscous forces in the system and result in early arrival times of the CO₂ plume at the leaky well [9].

We find that the risk of CO₂ leakage in excess of 0.123% could exceed 10% within the first two years of the simulation. However, this risk falls well below 5%, when we consider a leakage threshold of 0.227%. In our computation of optimum injection rate, we find that, given our assumed statistical distributions for the random inputs, an injection rate of 10.6 kg/s still ensures low risk of failure (defined as excess pressure buildup at the leaky well).

In our sensitivity analysis, we find that the balance of sensitivities changes as a function of time, where the CO₂ injection rate and porosity exhibit significant contribution to variance at early times, and become less important as the CO₂ plume reaches the leaky well. On the other hand, the reservoir permeability and leaky well permeability become dominant contributors to the variance of CO₂ leakage at later times. We also find that at early times the interactions among the different uncertain parameters has significant contribution to variance, but as the CO₂ plume reaches the leaky well, the bulk effect of interactions between the parameters to the variance is due to reservoir permeability and permeability of leaky well. The study of sensitivity of saturation to uncertain inputs in the three-dimensional domain reveals that the regions where porosity has a significant contribution to the variance travel with the fronts of the CO₂ plume; however, the reservoir permeability maintains a nearly constant dominant effect on variance within the regions with high CO₂ saturation.

7 Acknowledgement

Research reported in this publication was supported by the King Abdullah University of Science and Technology (KAUST) under the Academic Excellency Alliance (AEA) UT Austin-KAUST project "Uncertainty quantification for predictive modeling of the dissolution of porous and fractured media". Computational resources for the simulations presented in this publication have been made available by KAUST Research Computing and KAUST SuperComputing Lab. Bilal Saad is grateful for the support by the Saudi Arabia Basic Industries Corporation (SABIC). Bilal Saad, Serge Prudhomme, and Omar Knio are also participants of the KAUST SRI Center for Uncertainty Quantification in Computational Science and Engineering.

References

1. A. Alexanderian. On spectral methods for variance based sensitivity analysis. *Probability Surveys*, 10:51–68, 2013.
2. A. Alexanderian, O.P. Le Maître, H.N. Najm, M. Iskandarani, and O.M. Knio. Multiscale stochastic preconditioners in non-intrusive spectral projection. *Journal of Scientific Computing*, 50:306–340, 2012.
3. A. Alexanderian, J. Winokur, I. Sraj, A. Srinivasan, M. Iskandarani, W. C. Thacker, and O. M. Knio. Global sensitivity analysis in an ocean general circulation model: a sparse

- spectral projection approach. *Computational Geosciences*, 16(3):757–778, 2012.
4. I. Babuška, F. Nobile, and R. Tempone. A stochastic collocation method for elliptic partial differential equations with random input data. *SIAM J. Numer. Anal.*, 45(3):1005–1034, 2007.
 5. M. Batzle and Z. Wang. Seismic properties of pore fluids. *Geophysics*, 57:1396–1408, 1992.
 6. A. N. Brooks and A. T. Corey. Hydraulic properties of porous media. *Hydrol. pap. fort collins, Colorado State University*, 1964.
 7. C. Bryant, S. Prudhomme, and T. Wildey. Error decomposition and adaptivity for response surface approximations from pdes with parametric uncertainty. *SIAM/ASA Journal on Uncertainty Quantification*, 3(1):1020–1045, 2015.
 8. R. H. Cameron and W. T. Martin. The orthogonal development of non-linear functionals in series of fourier-hermite functionals. *Ann. Math.*, 48:385–392, 1947.
 9. H. Class, A. Ebigbo, R. Helmig, H. Dahle, J. N. Nordbotten, M. A. Celia, P. Audigane, M. Darcis, J. Ennis-King, Y. Fan, B. Flemisch, S. Gasda, M. Jin, S. Krug, D. Labregere, A. Naderi, R. J. Pawar, A. Sbair, G. T. Sunil, L. Trenty, and L. Wei. A benchmark-study on problems related to CO₂ storage in geologic formations. *Computational Geosciences*, 13:451–467, 2009.
 10. P. Conrad and Y. Marzouk. Adaptive Smolyak pseudospectral approximations. *SIAM J. Sci. Comput.*, 35(6):A2643–A2670, 2013.
 11. T. Crestaux, O.P. Le Maître, and J.-M. Martinez. Polynomial chaos expansion for sensitivity analysis. *Reliability Engineering & System Safety*, 94(7):1161 – 1172, 2009. Special Issue on Sensitivity Analysis.
 12. A. Ebigbo, H. Class, and R. Helmig. CO₂ leakage through an abandoned well: problem-oriented benchmarks. *Computational Geosciences*, 11(2):103–115, 2007.
 13. A. Feghhour, W. Wakeham, and V. Vesovic. The viscosity of carbon dioxide. *J. Phys. Chem. Ref. Data*, 27(1):31–44, 1998.
 14. B. Flemisch, M. Darcis, K. Erbertseder nad B. Faigle, A. Lauser, K. Mosthaf, S. Muthing, P. Nuske, A. Tatomir, M. Wolff, and R. Helmig. DUMUX: DUNE for Multi-{Phase, Component, Scale, Physics}, flow and transport in porous media. *Advances in Water Resources*, 34(9):1102–1112, 2011.
 15. IAPWS (The International Association for the Properties of Water and Steam). Release on the iapws industrial formulation 1997 for the thermodynamic properties of water and steam. <http://www.iapws.org/>. *Geophysics*, 1997.
 16. R.G. Ghanem and P.D. Spanos. *Stochastic Finite Elements: A Spectral Approach*. Dover, 2002. 2nd edition.
 17. J. Hampton and A. Doostan. Compressive sampling of polynomial chaos expansions: convergence analysis and sampling strategies. *J. Comput. Phys.*, 280:363–386, 2015.
 18. A. Hansson and M. Bryngelsson. Expert opinions on carbon dioxide capture and storage a framing of uncertainties and possibilities. *Energy Policy*, 37:2273–2282, 2009.
 19. T. Homma and A. Saltelli. Importance measures in global sensitivity analysis of nonlinear models. *Reliability Engineering & System Safety*, 52(1):1 – 17, 1996.
 20. R. Huber and R. Helmig. Node-centered finite-volume discretization for the numerical simulation of multiphase flow in heterogenous porous media. *Comput. Geosci.*, (4):141–164, 2000.
 21. A. Kopp, H. Class, and R. Helmig. Investigations on CO₂ storage capacity in saline aquifers - part 1: Dimensional analysis of flow processes and reservoir characteristics. *Int. J. of Green-house Gas Control*, 3:263–276, 2009.
 22. O.P. Le Maître and O.M. Knio. *Spectral Methods for Uncertainty Quantification With Applications to Computational Fluid Dynamics*. Scientific Computation. Springer, 2010.
 23. O.P. Le Maître, O.M. Knio, H.N. Najm, and R.G. Ghanem. Uncertainty propagation using Wiener-Haar expansions. *J. Comput. Physics*, 197(1):28–57, 2004.
 24. O.P. Le Maître, L. Mathelin, O.M. Knio, and M.Y. Hussaini. Asynchronous time integration for polynomial chaos expansion of uncertain periodic dynamics. *Discrete and Continuous Dynamical Systems*, 28(1):199–226, 2010.
 25. O.P. Le Maître, H.N. Najm, R.G. Ghanem, and O.M. Knio. Multi-resolution analysis of Wiener-type uncertainty propagation schemes. *J. Comput. Phys.*, 197(2):502–531, 2004.
 26. P. R. Maul, R. Metcalfe, J. Pearce, D. Savage, and J. M. West. Performance assessments for the geological storage of carbon dioxide: learning from the radioactive waste disposal experience. *International Journal of Greenhouse Gas Control*, 4(1):444–455, 2007.
 27. H. Nilsen, P. Herrera, M. Ashraf, I. Liggarden, M. Iding, C. Hermanrud, K. A. Lie, J. N. Nordbotten, H. Dahle, and E. Keilegavlen. Field-case simulation of CO₂ plume migration using vertical-equilibrium models. *Energy Procedia*, 4:3801–3808, 2011.
 28. J. N. Nordbotten, M. A. Celia, and S. Bachu. Analytical solutions for leakage rates through abandoned wells. *Water Resour. Res.*, 40(4):W04204, 2004.
 29. J. N. Nordbotten, M. A. Celia, and S. Bachu. Injection and storage of CO₂ in deep saline aquifers: analytical solution for CO₂ plume evolution during injection. *Transport in Porous Media*, 3:339–360, 2005.
 30. J. N. Nordbotten, M. A. Celia, S. Bachu, and H. Dahle. Semi-analytical solution for CO₂ leakage through an abandoned well. *Environmental science and technology*, 2:602–611, 2005.
 31. S. Oladyshkin, H. Class, R. Helmig, and W. Nowak. A concept for data-driven uncertainty quantification and its application to carbon dioxide storage in geological formations. *Advances in Water Resources*, 34:1508–1518, 2011.
 32. S. Oladyshkin, H. Class, R. Helmig, and W. Nowak. An integrative approach to robust design and probabilistic risk assessment for CO₂ storage in geological formations. *Computational Geosciences*, 15(3):565–577, 2011.
 33. C. Oldenburg. Screening and ranking framework for geologic CO₂ storage site selection on the basis of health, safety, and environmental risk. *Environmental Geology*, 54:1687–1694, 2008.
 34. C. Oldenburg, S.L. Bryant, and J.-P. Nicot. Certification framework based on effective trapping for geologic carbon sequestration. *Environmental Geology International Journal of Greenhouse Gas Control*, 4:444–457, 2009.
 35. J. Peng, J. Hampton, and A. Doostan. A weighted ℓ_1 -minimization approach for sparse polynomial chaos expansions. *Journal of Computational Physics*, 267:92–111, 2014.
 36. A. Saltelli. Sensitivity analysis for importance assessment. *Risk Analysis*, 22(3):579–590, 2002.
 37. I.M. Sobol. Estimation of the sensitivity of nonlinear mathematical models. *Matematicheskoe Modelirovanie*, 2(1):112–118, 1990.

38. I.M Sobol. Global sensitivity indices for nonlinear mathematical models and their monte carlo estimates. *Mathematics and Computers in Simulation*, 55(1-3):271 – 280, 2001. The Second IMACS Seminar on Monte Carlo Methods.
39. R. Span and W. Wagner. A new equation of state for carbon dioxide covering the fluid region from the triple-point temperature to 1100 K at pressures up to 800 MPa. *J. Phys. Chem. Ref. Data*, 25(6):1509–1596, 1996.
40. N. Spycher and K. Pruess. Co₂-h₂O mixtures in the geological sequestration of co₂. ii. partitioning in chloride brines at 12-100 °C and up to 600 bar. *Geochim. Cosmochim. Acta*, 69(13):3309–3320, 2005.
41. B. Sudret. Global sensitivity analysis using polynomial chaos expansions. *Reliability Engineering & System Safety*, 93(7):964 – 979, 2008.
42. A. Y. Sun, M. Zeidouni, J. P. Nicot, Z. Lu, and D. Zhang. Assessing leakage detectability at geologic co₂ sequestration sites using the probabilistic collocation method. *Advances in Water Resources*, 56:49–60, 2013.
43. L. Walter, P. J. Binning, S. Oladyshkin, Bernd Flemisch, , and H. Class. Brine migration resulting from co₂ injection into saline aquifers- an approach to risk estimation including various levels of uncertainty. *International Journal of Greenhouse Gas Control*, 9:495–506, 2012.
44. N. Wiener. The Homogeneous Chaos. *Amer. J. Math.*, 60:897–936, 1938.
45. D. Williams. *Probability with martingales*. Cambridge Mathematical Textbooks. Cambridge University Press, Cambridge, 1991.
46. J. Winokur, P. Conrad, I. Sraj, O. M. Knio, A. Srinivasan, W. C. Thacker, Y. Marzouk, and M. Iskandarani. A priori testing of sparse adaptive polynomial chaos expansions using an ocean general circulation model database. *Comput. Geosci.*, 17(6):899–911, 2013.
47. D. Xiu, D. Lucor, C.H. Su, and G.E. Karniadakis. Stochastic modeling of flow structure interactions using generalized polynomial chaos. *J. Fluids Engrg*, 124:51–59, 2002.
48. D.B. Xiu and G.E. Karniadakis. The Wiener-Askey Polynomial Chaos for stochastic differential equations. *SIAM J. Sci. Comput.*, 24:619–644, 2002.
49. D.B. Xiu and G.E. Karniadakis. Modeling uncertainty in flow simulations via generalized Polynomial Chaos. *J. Comput. Phys.*, 187:137–167, 2003.
50. L. Yan, L. Guo, and D. Xiu. Stochastic collocation algorithms using ℓ_1 -minimization. *Int. J. Uncertain. Quantif.*, 2(3):279–293, 2012.
51. Q. Zhou, J. T. Birkholzer, C. F. Tsang, and J. Rutqvist. A method for quick assessment of co₂ storage capacity in closed and semi-closed saline formations. *International Journal of Greenhouse Gas Control*, 2:626–639, 2008.